

Structure and motion of junctions between coherent and incoherent twin boundaries in copper

J.A. Brown, N.M. Ghoniem*

Mechanical and Aerospace Engineering, University of California, Los Angeles, CA 90095, USA

Received 28 April 2009; received in revised form 4 June 2009; accepted 6 June 2009

Available online 4 July 2009

Abstract

The atomic mechanisms of twin boundary migration in copper under externally applied mechanical loads and during thermal annealing are investigated utilizing molecular dynamics computer simulations. The migration dynamics of the incoherent $\Sigma = 3[110](112)$ twin boundary (ITB), pinned between two $\Sigma = 3[110](111)$ twin boundaries, is determined. A three-dimensional structural model is described for the junction between intersecting coherent and incoherent twin boundaries, and migration velocities are calculated under thermal annealing conditions. It is shown that the coherent twin boundary (CTB)/ITB junction results in breaking the crystal symmetry by creation of either an edge dislocation or a mixed (edge/screw) at the intersection. These two types of defects can lead to pronounced differences in the observed migration (and hence annealing) rates of ICT/CTB junctions. The annealing rate resulting from the migration of ITBs with a mixed dislocation is found to be more than twice that of the edge dislocation. The mechanism of ITB motion is shown to be governed by successive kink-like motion of neighboring atomic columns, each of which is shifted by $1/4[110]$, followed by structural relaxation to accommodate boundary motion.

© 2009 Acta Materialia Inc. Published by Elsevier Ltd. All rights reserved.

Keywords: Copper; Crystal structure; Interface migration; MD simulations; Twinning

1. Introduction

Grain boundaries play a vital role in controlling the bulk mechanical properties of polycrystalline materials [1]. One special type of grain boundary – the twin boundary – has always been of particular interest because of the role it plays in deformation processes [2,3]. Moreover, the influence of twin boundaries on material deformation has recently received a renewed level of interest with the development of nanotwinned copper, a newly discovered nanostructure that engineers nanograined copper with ultrahigh-density twins [4]. Recent experiments have shown that the high density of nanoscale growth twins in fine-grained Cu dramatically elevates the strength while providing considerable tensile ductility [4–7]. In order to determine the influence of twin boundaries on the mechanical

deformation of nanotwinned copper, it is vital to establish an understanding of the atomistic mechanisms that govern twin boundary motion. The interest here is on the role of the $\Sigma 3$ boundary in copper, which results in an face-centered cubic (fcc) structure from either a twist or tilt operation of one part of the crystal (upper) with respect to another (lower). The twist reconstruction involves cutting the crystal along a $\{111\}$ plane and rotating the upper part by 180° or 60° around the $[111]$ -axis. Alternatively, one can achieve the same configuration by a tilt operation, in which the crystal is cut along a $\{111\}$ plane and the upper part is then rotated by a misorientation angle $\theta = 70.53^\circ$ around the $\langle 110 \rangle$ direction. For the same θ , two additional degrees of freedom still exist between the adjacent crystals, and these can be assigned to two angles describing the rotation of one grain boundary (GB) crystal plane relative to the other. The first is the inclination angle, Φ , which describes the relative rotation of the two planes about the common tilt axis, while the second, Ψ , is an angle that

* Corresponding author.

E-mail address: ghoniem@ucla.edu (N.M. Ghoniem).

describes the relative twist. For the symmetric coherent twin boundary (CTB), $\Phi = 0$ and $\Psi = 0$, while $\Phi = 90^\circ$ and $\Psi = 0$ for the symmetric incoherent twin boundary (ITB).

The objective of this paper is to investigate the structure and migration mechanism of the ITB when it is pinned between two CTBs in copper, and to shed light on the relationship between the ITB/CTB junction structure and the rate of ITB thermal annealing. Since twin boundaries are essentially defects in the crystal structure, they are not expected to be absolutely stable under applied loads or at high temperature, and their motion would lead to shape change and significantly impacts the plasticity of nanostructured materials containing twins. ITBs ($\Sigma = 3[110](112)$) are often observed to terminate in between CTBs ($\Sigma = 3[110](111)$), and hence junctions between these two types of boundaries must form. The three-dimensional geometry and stability of these junctions are of interest, because the motion of ITBs under thermal annealing conditions can result in removal of desirable twinned structures in copper.

The relationship between twin boundaries and deformation, and the migration of twin boundaries, have recently been the subject of experimental and computational investigations. Frøseth, et al. discussed the presence of grown-in twins in nanocrystalline Al and concluded that the mechanism of twin migration enhanced plastic deformation [8]. In their investigation of twinning mechanisms, Frøseth, et al. used molecular dynamics (MD) simulations and general planar fault energy curves to demonstrate that twinning can occur by means of partial dislocations nucleating at nanocrystalline grain boundaries [9]. The motion of twin boundaries was also experimentally investigated by Kizuka, who observed that shearing of nanometer-sized gold contacts induced not only sliding of twin boundaries, but also simultaneous boundary migration [10]. Likewise, Field et al. [11] observed the migration of copper twin boundaries during deformation, and produced evidence using channel die deformation and imaging to support their conclusion that twin boundaries can serve as sources of dislocations. Using in situ transmission electron microscopy, Wang et al. [12] observed the dynamic process of twin boundary migration in Cu containing nanoscale twins. They provide direct evidence of twin boundary migration via Shockley partial dislocation emission from twin boundary/grain boundary intersections. Medlin et al. [13] presented a study of the structure and migration mechanisms of ITBs in aluminum, where both high-resolution transmission electron microscopy (HRTEM) and atomistic simulations were employed to examine the migration process. Inkson and Humphreys [14] used high-resolution electron microscopy to examine the perpendicular junction between ITBs and CTBs in γ -TiAl grains, and observed the migration of the ITB by passage of partial dislocations.

The structure and stability of junctions between CTBs and ITBs are also important, because junction motion

can significantly affect the concentration of twin boundaries in nanotwinned copper [15]. Marquis, et al. [16] studied the junction of an incoherent and coherent twin boundary in gold – a low-energy stacking fault material like copper, and noted the variations in crystal structure across these boundaries. Medlin et al. [17] performed HRTEM observations of the $\Sigma = 3[0\bar{1}\bar{1}]$ boundary in Al and showed that the glide of dissociated $a/3[111]$ grain boundary dislocations on the incoherent twin are incorporated into the growing coherent twin lamella. Tschopp and McDowell [18] showed a structural dependence of the family of $\Sigma = 3[110]$ GBs on the inclination angle, and showed that the faceting of asymmetric TBs in Cu and Al intermediate to the symmetric CTB and ITB can be completely defined in terms of structural units (SUs) for these two symmetric boundaries. Unlike the CTB, in order for an isolated ITB to arrive at its lowest energy configuration, the symmetry must be broken by rigid body translations of adjacent grains [19]. Furthermore, the ITB dissociates into a high-angle boundary and a low-angle boundary [20]. It has been shown that externally applied $\langle 111 \rangle$ type shearing of an ITB results in migration of the low-angle boundary while the high-angle boundary remains fixed. The result of this process is an extension of the stacking faults into the bulk, associated with an expansion of the 9R phase with no net migration of the ITB [21]. Marquis et al. [16] examined the structural character of an ITB of finite length pinned between to ITB/CTB junctions, and noted that rigid body translations in $\langle 111 \rangle$ directions characteristic of this boundary were affected by its finite length, and that closely interacting ITB/CTB junctions served to stabilize a stacking fault extending between them. Pénisson, et al. [22] described the structure of the ITB in Al, and observed no lateral shift in the grains resulting in a symmetric boundary structure for the ITB. Medlin et al. [13] used experimental HRTEM observations coupled with atomistic simulations of a symmetric ITB in Al to describe the migration dynamics of an ITB/CTB junction. Recently, several experimental studies indicated that nano-twins can play a significant role in stabilizing grain boundaries. Chen et al. [23] made experimental observations of atomic diffusion at twin-modified grain boundaries, and concluded that, as a result of the incubation time of a new step nucleation, the triple point where a twin boundary meets a grain boundary slows down grain boundary and surface electromigration by one order of magnitude. Saldana et al. [24] showed that the thermal stability of nanostructured materials is significantly improved when a dense dispersion of nanotwins is introduced. While these studies have revealed aspects of the structure and motion of ITBs and CTBs in several fcc metals, the detailed structure of ITB/CTB junctions and the relationship of this structure to the migration of ITBs at high temperature have not been determined.

The objective of the present work is to utilize MD simulations in order to examine the structure and migration mechanisms of ITBs in copper under externally applied mechanical loads and during thermal annealing. The

mobility of an ITB in terms of “junction drag” may be viewed in the broader context of the influence of junctions on grain boundary mobility [25,26]. First, the computational procedure and numerical methods used in MD simulations are describe in Section 2. Section 3 will furnish the ground state structures of the two symmetric $\Sigma = 3$ twin boundaries, as well as present two metastable structures for the incoherent twin boundary that will be relevant to the discussion in Section 4, where we turn our attention to the structure and dynamics of ITB/CTB junctions, focusing on the influence of temperature and applied stress. Atomistic and dislocation mechanisms associated with junction motion are also presented. Finally, a summary of the present work and conclusions are given in Section 5.

2. Computer simulation procedures

An embedded-atom method potential constructed by fitting to experimental and first-principles data [27] was used to determine interaction forces and energies in MD simulations, which were performed using the ITAP Program [28].

In order to simulate an ITB/CTB junction, an orthorhombic simulation block was first constructed whose axes were aligned along the $[\bar{1}11]$, $[1\bar{1}2]$ and $[110]$ directions, as shown in Fig. 1. First, a geometric construction was used to create the initial structure of a twinned crystal embedded in the original fcc structure, and bounded by two CTBs and one ITBs. An fcc copper crystal with the $\{111\}$ -stacking labelled as ABCABC... and the $\{1\bar{1}2\}$ -stacking labelled as XYZUVWXYZUVW... is shown in Fig. 1a, while Fig. 1b shows a sketch of intermediate rotation of a prismatic block about the $[110]$ -axis. The final configuration of the block and corresponding plane stacking after rotation with an angle of 2π about $[110]$ is shown in Fig. 1c.

The final geometric configuration, which serves as the initial configuration for MD simulations, is shown in Fig. 1d, where the coordinate axes for the crystal and twinned region are indicated. Periodic boundary conditions are imposed on the (110) and $(1\bar{1}1)$ faces. v_{GB} is the velocity of the migrating ITB and the arrow indicates the direction of migration. The entire simulation volume was 22.3 nm in the $[\bar{1}11]$ -direction, 32.6 nm in the $[1\bar{1}2]$ -direction,

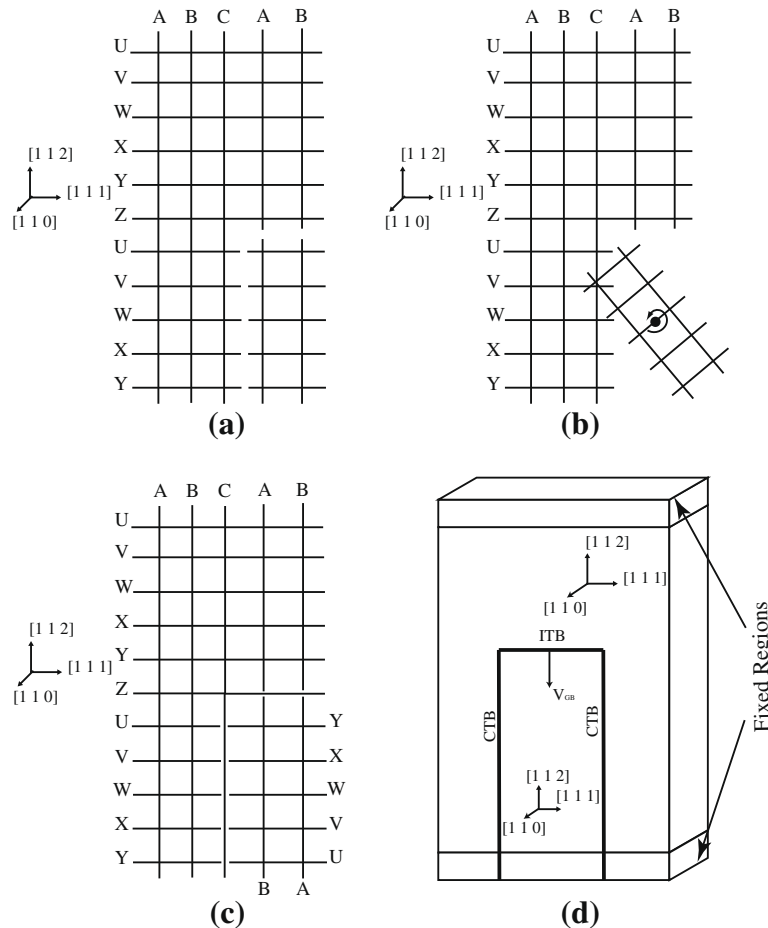


Fig. 1. Schematic of an ITB/CTB junction simulation block geometry: (a) fcc copper crystal with the $\{111\}$ -stacking labeled as ABCABC... and the $\{112\}$ -stacking labeled as XYZUVWXYZUVW...; (b) intermediate rotation of a prismatic block about the $[110]$ -axis; (c) final configuration after rotation with an angle of 2π about $[110]$; and (d) simulation block showing the twinned region bounded by one ITB and two CTBs. The coordinate axes for the crystal and twinned region are indicated. Periodic boundary conditions are imposed on the (110) and $(\bar{1}11)$ faces. v_{GB} is the velocity of the migrating ITB and the arrow indicates the direction of migration.

tion and 3.0 nm in the [110]-direction, and contained 200,000 atoms. The segment of ITB pinned between the two junctions is 15.7 nm wide. The ITB was initially constructed at a sufficient distance from the upper fixed region such that the ITB and junctions experienced the equivalent of bulk interactions. The atomic positions were then relaxed statically, followed by slowly raising the temperature stepwise to 1000 K over a span of 1 ns. In directions normal to the TB, the grains were terminated by fixed boundary conditions, which were imposed by creating thin slabs of fixed atoms at the top and bottom of the simulation block. These thin slabs were allowed to interact with their neighbors, but the atoms in the thin slabs were regarded as a single unit. MD simulations were performed in the canonical (NVT) ensemble, using a constant-temperature Nosé–Hoover-type thermostat. Prior to beginning an MD simulation, the computational block was subjected to a uniform expansion corresponding to the chosen temperature. This a priori process takes into account the thermal expansion that would take place naturally, and so maintains the simulation block at zero average pressure. The thermal expansion factors were determined by Mishin et al. [27] using zero-pressure Monte Carlo simulations.

The symmetric $\Sigma 3$ ITB boundary created geometrically by the crystal rotation operation is in fact a high-energy boundary, and the energy can be reduced if the symmetry is broken by nucleation of a defect. We thus need to determine the minimum energy structure of these boundaries by

applying rigid body translations to the twinned block while fixing the atomic positions of the surrounding crystal and then relaxing the structure statically at 0 K by minimizing the total potential energy via the conjugate gradient method. This method allows determination of the minimum energy configuration of a variety of metastable translated states for the ITB, as will be discussed in the next section.

3. Minimum energy twin boundary structures

Fig. 2 shows calculated stable and metastable structures for the coherent (Fig. 2a) and incoherent (Fig. 2b–d) twin boundaries, with their corresponding GB energies, γ_{GB} . The $\Sigma = 3$ CTB shown in Fig. 2a is a highly symmetric, low-energy grain boundary that has been well documented [1]. The ITB offers a much more complex atomic structure, and in Fig. 2d the lowest energy structure for the ITB in copper is shown [29,30]. This represents a shifted structure wherein the symmetry has been broken by rigid body translation of the two half-grains against one another (a dislocation creation operation). Further relaxation of this boundary beyond the rigid body translation has resulted in a dissociated structure forming a layer of 9R phase terminated by a periodic array of double-core and 30° Shockley partial dislocations [21], positioned on every third close-packed plane and terminating the “stacking faults” on one side of the 9R layer. On the other side, an array of 90° pure

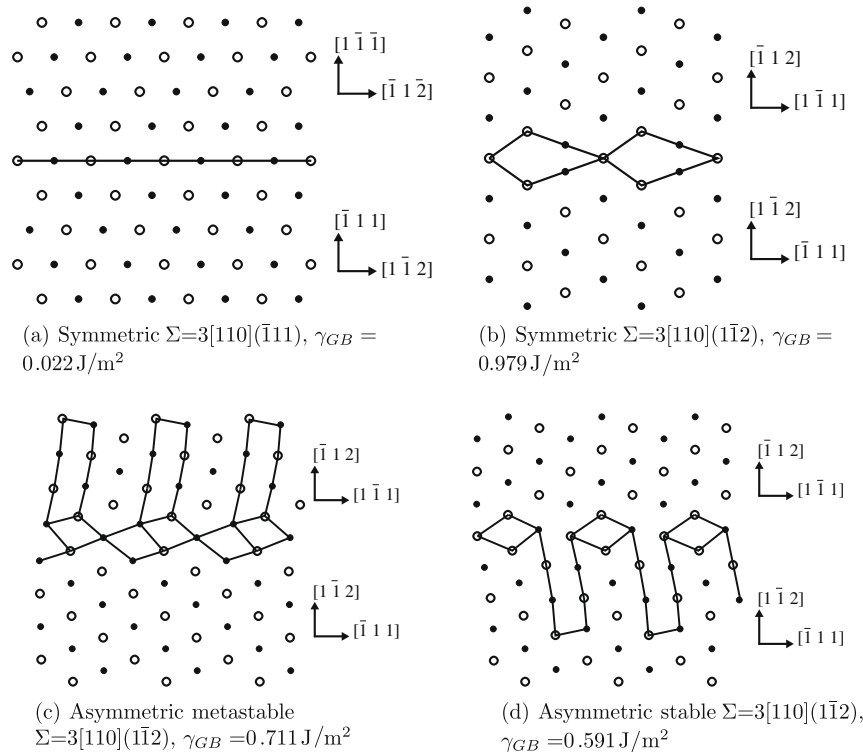


Fig. 2. Calculated boundary structures and energies (γ_{GB}) for coherent (a) $\Sigma = 3[110](\bar{1}11)$ twin boundary and incoherent (b–d) $\Sigma = 3[110](\bar{1}12)$ twin boundaries. All boundaries are projected along the [110] tilt axis. The structural units for the boundaries are outlined. The black dots and white circles indicate two separate [220] planes.

edge Shockley partial dislocations forms a low-angle tilt boundary, consistent with analysis of the 9R layer structure in many low stacking fault energy materials [20,21,31,32].

In addition to the two minimum energy structures for the CTB and ITB, two metastable structures for the ITB are also shown in Fig. 2b and c. The symmetric form of the ITB in Cu is not the preferred or lowest energy configuration for this boundary, however, and there must be some significant displacement of the two half-grains against one another in order to arrive at the lowest energy configuration (Fig. 2d). This can be accomplished by static relaxation algorithms (e.g. conjugate gradient methods), aided by rigid body displacements of the grains against one another. Rigid body displacement of one half-grain by $\mathbf{b}_A = \frac{a}{4}[\bar{1}\bar{1}0] + \frac{a}{6}[1\bar{1}\bar{1}]$ will result in placing the boundary in a the lowest energy configuration [33,14,34]. However, this shear displacement is a symmetry breaking operation, and can result from the nucleation of a Type-A junction dislocation of \mathbf{b}_A , composed of a partial screw dislocation, and a partial Frank-type edge dislocation. Fig. 2c is the result of relaxing an ITB without the edge component of \mathbf{b}_A , which is clearly a higher energy configuration and will thus not be pursued further. Another method of symmetry breaking is by removing the Y-plane shown in Fig. 1, which terminates at the CTB. This second operation corresponds to the nucleation of a Type-B negative Frank partial dislocation at the junction, and can glide on the CTB plane with $\mathbf{b}_B = \frac{a}{6}[\bar{1}12]$. The asymmetric ITB energy still remains the same as shown in Fig. 2d (0.59 J m^{-2}), because the end stacking across the ITB is the same as with a Type-A dislocation. These energy calculations suggest that the minimum energy ITB configuration, when joined to a neighboring CTB, must restructure by creating either Type-A or Type-B junction dislocation. We will next investigate the stability and motion of the ITB under thermal annealing conditions because of its relevance to the overall stability of nanotwinned copper crystals at high temperatures.

4. Motion of ITB/CTB junctions

We discuss here the mechanisms of TB boundary migration, since HRTEM observations indicate that ITB/CTB junctions are mobile at temperature [15]. Considering the ITB/CTB junction structure as the intersection between plane stacking, as shown in Fig. 3, and allowing a U-plane to adjoin a YZ-plane across the CTB junction will result in a symmetric ITB, which is a high energy structure and is unstable (Fig. 2). Thus, the stacking sequence will have a driving force to change to VWXY|Z|XWVU, a lower energy structure. However, forcing a U-plane to adjoin an X-plane across the CTB interface and continuing the sequence as shown will break the symmetry of the CTB and will result in the equivalent stacking of close-packed ($\bar{1}\bar{1}1$) planes to produce the sequence ABCCBA, a highly unstable stacking sequence for the CTB. Thus, in order to produce such a twin boundary junction, this seeming discontinuity must be accounted for by Type-A or Type-

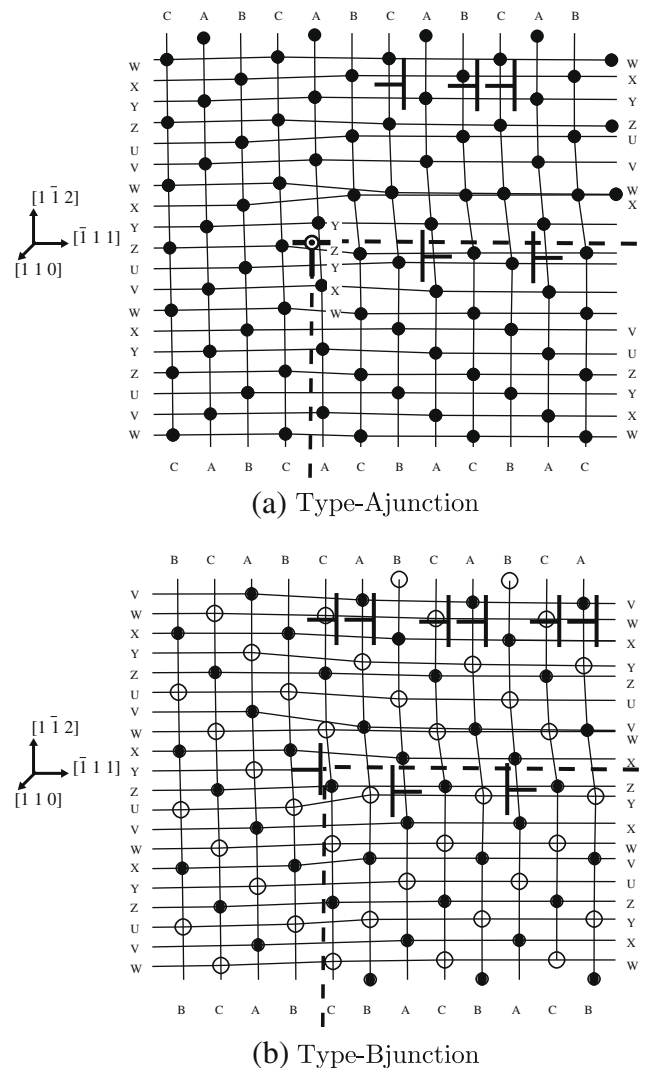


Fig. 3. Schematic of the ITB/CTB junction as stacking of $(1\bar{1}\bar{2})$ and $(\bar{1}\bar{1}1)$ planes. Junction dislocations are shown at the ITB/CTB corner. Note that the CTB plane is intrinsic (B) in Type-A, while it is extrinsic (C) in Type-B.

B dislocations, as shown in Fig. 3. The results of these atomic structures will be shown to lead to drastically differing migration rates.

The atomic structure of Type-A CTB/ITB junction is shown in Fig. 4, where the structural units are outlined. Atoms are colored continuously according to their position in the $[1\bar{1}0]$ direction (screw direction of junction dislocation), progressing from red to blue, where red atoms are nearest the viewer, while blue atoms are the furthest. The screw component of the junction dislocation results in helical atomic arrangements near the junction. When the U-plane adjoins the X-plane at the ITB interface, the crystal is forced to strain towards the X-plane position away from the junction, as is apparent from color progression from orange to green to blue across the ITB. An arc is formed, beginning at the junction and extending around the ITB on both sides. Beyond this arc the lattice is no longer strained. The simple planar projection of SUs comprising

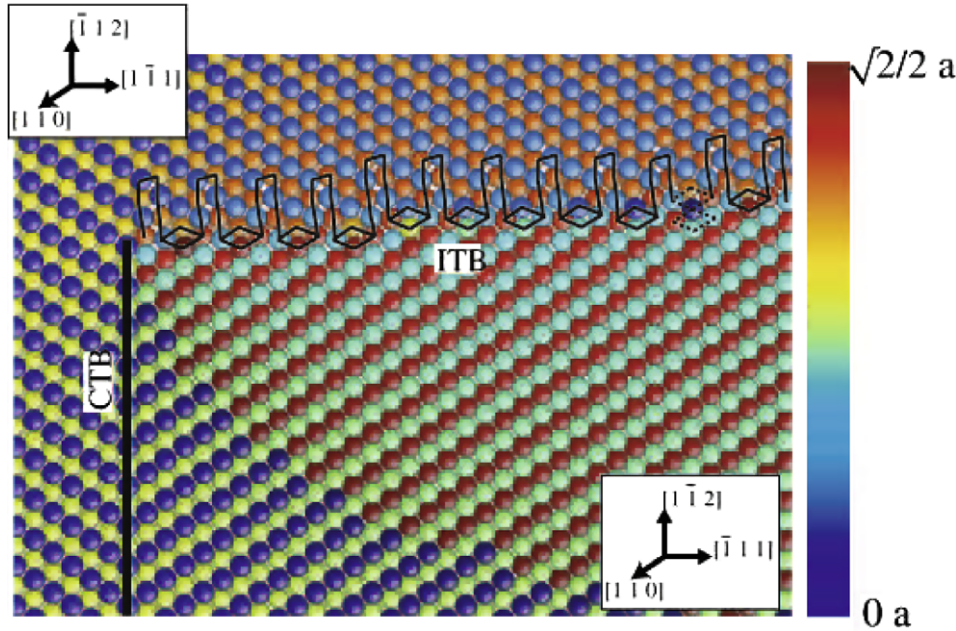


Fig. 4. Simulation results for the atomic structure of a Type-A ITB/CTB junction. The boundary junction is projected along the $[110]$ tilt axis and the structural units of the individual boundaries are outlined. The atoms are colored according to their position in the $[110]$ direction (normal to the page) progressing from blue (nearest the viewer) to red (farthest) [35]. (For interpretation of the references to colour in this figure legend, the reader is referred to the web version of this article.)

the 9R phase of an ITB (shown in Fig. 2) is consistent with the dislocation array model, where the SUs are negative edge Shockley partials on one side of the 9R phase (lower in Fig. 3) and positive double core 30° partials on the other side of a stacking fault. The colors indicate that the units are tilted either towards or away from the viewer as a result of Type-A junction dislocation, consistent with the strain field generated by a dislocation with $\mathbf{b}_A = \frac{a}{4}[\bar{1}\bar{1}0] + \frac{a}{6}[1\bar{1}\bar{1}]$.

Now that the structure of a Type-A junction is established, we next consider construction of the Type-B junction. It is possible to generate an identical infinite ITB within a supercell by removing a single $\{112\}$ plane at the twin boundary and performing an additional rigid body shift of the grains towards one another by $\sqrt{6}a$ to eliminate the space left behind. This approach results in a structurally identical twin boundary to that produced using the rigid body translation of the Type-A junction, with no screw dislocation component at the junction. Constructing such an ITB within a supercell using either the latter or the prior approach makes no difference for an infinitely large twin boundary. However, when dealing with a finite boundary pinned between boundary junctions, no screw component is introduced at the junction. Referring to Fig. 3, if the Y-plane is manually removed and the boundary positions are then allowed to slowly relax, the result is a CTB with an additional Frank partial dislocation of Burgers vector $\mathbf{b}_B = \frac{1}{6}[1\bar{1}2]$. However, now the Z-plane can be stacked on top of the X-plane forming the ITB with no rigid body shift in the $[110]$ direction required.

The influence of an applied shear stress on junction motion is first considered. Under an applied shear along

$\langle 111 \rangle$ directions, an ITB expands the 9R phase into the bulk, where the double core Shockley partials pin the boundary from one side. This expansion is a reversible process, mediated by the motion of the 90° Shockley partial dislocations, and results in reversible plastic strain. An applied shear in the $\langle 110 \rangle$ directions results only in grain boundary sliding, and decoupling between ITB sliding and transverse migration of Shockley partial dislocations is observed as the shear approaches any of the $\langle 110 \rangle$ directions.

Since the ITB/CTB junction is a high-energy configuration, it is expected that the motion is a thermally activated process that results in energy minimization by coarsening of the grains at elevated temperatures. MD simulations were performed at a constant temperature of 1000 K for 8 ns, and Fig. 5a and b show plots of the positions of the ITB as a function of time, for Type-A and Type-B junctions, respectively. The position of the ITB was measured at the two extremes of the 9R phase, and their average. The three curves clearly show correlated motion as the boundary migrates, so while the boundary does not shift as a single unit, it moves stepwise from one side to the other. The dashed lines are linear interpolations of the three curves. The results indicate that the average speed of an ITB boundary with Type-A junction dislocation is 1.17 m s^{-1} , while that of Type-B junction is considerably slower (0.51 m s^{-1}).

A simple atomistic model of the migration mechanism for the CTB/ITB junctions is shown in Fig. 6, which is appropriate to low stacking fault energy metals (for a local twinning mechanism in higher stacking fault metals, see

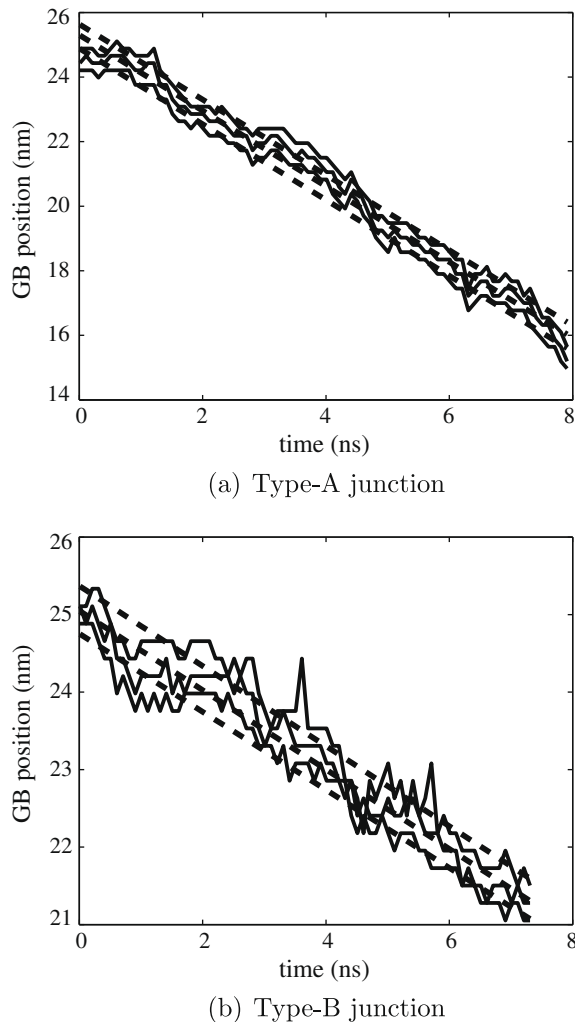


Fig. 5. Time dependence of the position of a $\Sigma=3$ incoherent twin boundary (ITB) pinned between two coherent twin boundaries at a temperature $T=1000$ K for a Type-A junction (a) and a Type-B junction (b). The three lines indicate positions of the double core and edge Shockley partials of the dissociated ITB, with the average position given by the middle line.

Ref. [13]). The figure shows a time progression of ITB migration for Type-A junctions, where the dark outline shows the SUs in their current positions, whereas the dashed lines indicate where the SUs will be at the next step. The two different colors, white and black, are for atomic positions at varying heights in the $[110]$ -direction. Focusing first on Fig. 6a, one can see the initial, flat ITB extending horizontally. The intrinsic stacking faults are outlined extending out of the boundary. The CTB is delineated by the single line extending vertically down. For one step of the migration to take place, the diamond-shaped structural unit adjoining the CTB must move down as indicated by the dashed lines. This is accomplished simply by having the single column of atoms represented by the white circle at the bottom of the diamond structural unit shift by $a/4[\bar{1}\bar{1}0]$. This shift is represented by changing the color of the point from white to black, as shown in Fig. 6b. Some slight structural relaxations then occur as the boundary

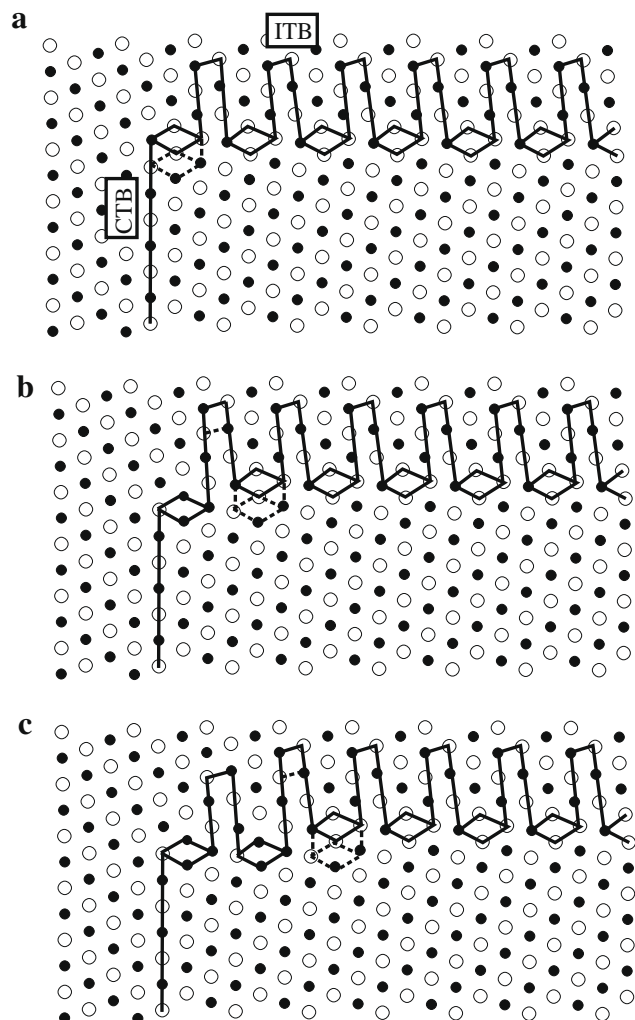


Fig. 6. Diagram of the atomic migration mechanism of twin boundary junctions. The dark lines indicate the current structural units and the dashed indicate the positions where structural units will shift after the boundary migration takes place. (a) The initial boundary. The first step is shown occurring in (b) and continues to propagate in (c). This step then moves across the boundary and is repeated.

plane adjusts downward. This process is then repeated on the adjacent diamond unit, as shown in Fig. 6b. The atomistic mechanism outlined here propagates the length of the ITB until it reaches the other boundary junction, resulting in a single transverse atomic step. However, a single step (entire column of atoms) does not need to complete throughout the boundary before the next step can begin to propagate, because of kink nucleation along dislocation lines, resulting in superimposed stochastic fluctuations on top of continuous junction motion. For Type-B junctions, the overall result is the same as the boundary migrates down. However, the absence of a screw component of the junction dislocation results in more fluctuations in the ITB position, as can be seen in the figure.

An equivalent description is that based on the motion of dislocation arrays bounding the ITB 9R phase. In a Type-A junction, the edge component of the ITB/CTB junction dislocation must climb on the CTB plane. The screw com-

ponent then drags the nearest 90° 9R partial, which then glides on $\{111\}$ -planes. An effective force is generated on the next nearest double core Shockley partials through the action of the stacking fault within the 9R region. The process repeats by successive motion of double core/pure edge dislocation pairs from one CTB boundary to the opposite one. The dislocation mechanism in Type-B is the glide of the junction Frank partial dislocation on the CTB plane, dragging the 9R phase Shockley partials along their successive glide planes. In both cases, dislocation motion is controlled by double kink nucleation and propagation along dislocation cores.

5. Summary and conclusions

The current investigation is focused on the structure and migration mechanisms of twin boundaries in copper, where we use MD simulations to determine the most likely structure of incoherent twin boundaries in copper, and their response to applied external stress or temperature. Of particular interest is the atomic structure of the junction formed between ITBs and CTBs, because the thermal stability of twins in copper is dependent on the strength of this junction and its response to thermal annealing. The following conclusions can be drawn from the present work.

1. Under an applied shear strain along $\langle 111 \rangle$ directions, an ITB reacts by expanding the 9R phase into the bulk through the motion of 90° Shockley partials. An applied strain in $\langle 110 \rangle$ directions is found to result only in grain boundary sliding, and a decoupling between ITB sliding and transverse migration of Shockley partial dislocations is observed as the shear approaches any of the $\langle 110 \rangle$ directions.
2. An ITB can be represented by a reversal of the stacking sequence of the six $(1\bar{1}2)$ planes, denoted by UVW-XY|Z|YXWVU. The lowest energy structure for an ITB can be achieved by stacking the $(1\bar{1}2)$ planes as UVWXY|Z|XWVU, which can be realized by either the prescribed rigid body shift (Type-A junction), or by removing an atomic plane at the GB (Type-B junction).
3. The simulated structure of the ITB/CTB interface junction is complex. The migration of these junctions when enclosing a grain was determined to be a thermally activated process that can lead to coarsening of grains containing twinned nanostructures.
4. The presence of a screw component of the ITB/CTB junction dislocation can lead to pronounced differences in the observed migration rates of ITB/CTB junctions. The annealing rate resulting from the migration of ITBs with a $[110]$ partial screw dislocation is more than twice that when the junction does not contain this component.
5. The migration mechanism of ITBs, and hence the annealing behavior of nanotwinned copper, has been shown to be initiated from the need to reduce the overall energy of the system by eliminating junctions between

ITBs and CTBs. This is achieved by successive kink-like motion of neighboring atomic columns, each of which is shifted by $1/4[110]$, followed by structural relaxation to accommodate boundary motion. Shockley partial dislocations terminating the 9R phase at the ITB boundary are dragged down along with the migrating boundary. Depending on temperature and the size of the enclosed twinned crystal, single (for small-size) or multiple (for large-size) kinks may exist along the ITB at any given time.

6. ITB migration rates showed a very strong dependence upon the temperature of the simulation, increasing with increasing temperature, as well as an inverse dependence on the width of the ITB segment.

Acknowledgements

This work was supported by the National Science Foundation Grants, Numbers 0506841 and 0625299 with UCLA.

References

- [1] Sutton AP, Balluffi RW. *Interfaces in crystalline materials*. Oxford: Oxford Science Publ.; 1995.
- [2] Christian JW, Mahajan S. *Prog Mater Sci* 1995;39:1.
- [3] Wolf D, Yamakov V, Phillpot SR, Mukherjee A, Gleiter H. *Acta Mater* 2005;53:1.
- [4] Lu L, Shen Y, Chen X, Qian L, Lu K. *Science* 2004;304:422.
- [5] Ma E, Wang YM, Lu QH, Sui ML, Lu L, Lu K. *Appl Phys Lett* 2004;85:4932.
- [6] Zhao WS, Tao NR, Guo JY, Lu QH, Lu K. *Scripta Mater* 2005;53:745.
- [7] Zhu T, Samanta A, Kim HG, Suresh S. *Proc Nat A Sci* 2007;104:3031.
- [8] Frøseth AG, Swygenhoven HV, Derlet PM. *Acta Mater* 2004;52:2259.
- [9] Frøseth AG, Derlet PM, Swygenhoven HV. *Adv Eng Mater* 2005;7:16.
- [10] Kizuka T. *Jpn J Appl Phys* 2007;46(11):7396.
- [11] Field DP, True BW, Lillo TM, Flinn JE. *Mater Sci Eng A* 2004;372:173.
- [12] Wang YB, Sui ML, Ma E. *Philos Mag Lett* 2007;87(12):935.
- [13] Medlin DL, Stobbs WM, Weinberg JD, Angelo JE, Daw MS. *Mater Res Soc Symp Proc* 1994;319:273.
- [14] Inkson BJ, Humphreys CJ. *Philos Mag A* 1996;73:1647.
- [15] Zhang X, Tu KN, Chen Z, Tan YK, Wong CC, Mhaisalkar SG, et al. *J Nanosci Nanotech* 2008;8:2568.
- [16] Marquis EA, Hamilton JC, Medlin DL, Léonard F. *Phys Rev Lett* 2004;93:156101.
- [17] Medlin DL, Carter CB, Angelo JE, Mills MJ. *Philos Mag A* 1997;75:733.
- [18] Tschopp M, McDowell D. *J Mater Sci* 2007;42(18):7806.
- [19] Carter CB, Medlin DL, Angelo JE, Mills MJ. *Mater Sci Forum* 1996;207-209:209.
- [20] Medlin DL, Campbell GH, Carter CB. *Acta Mater* 1998;46:5135.
- [21] Campbell GH, Chan DK, Medlin DL, Angelo JE, Carter CB. *Scripta Mater* 1996;35:837.
- [22] Pénisson JM, Dahmen U, Mills MJ. *Philos Mag Lett* 1991;64:277.
- [23] Chen K-C, Wu W-W, Liao C-N, Chen L-J, Tu KN. *Science* 2008;321(5892):1066.
- [24] Saldana C, Murthy TG, Shankar MR, Stach EA, Chandrasekar S. *Appl Phys Lett* 2009;94:021910.

- [25] Gottstein G, Shvindlerman LS. *Acta Mater* 2002;50(4):703.
- [26] King A. *Interface Sci* 1999;7:251.
- [27] Mishin Y, Mehl MJ, Papaconstantopoulos DA, Voter AF, Kress JD. *Phys Rev B* 2001;63:224106.
- [28] Stadler J, Mikulla R, Trebin HR. *Int J Mod Phys C* 1997;8:1131.
- [29] Wolf U, Ernst F, Muschik T, Finnis MW, Fischmeister HF. *Philos Mag A* 1992;66:991.
- [30] Tschopp MA, McDowell DL. *Philos Mag* 2007;87:1–27.
- [31] Ernst F, Finnis MW, Hofmann D, Muschik T, Schonberger U, Wolf U. *Scripta Mater* 1996;35:837.
- [32] Rittner JD, Seidman DN, Merkle KL. *Phys Rev B* 1996;53:4241.
- [33] Angelo JE, Baskes MI. *Interface Sci* 1996;4:47–63.
- [34] Pond RC, Vitek V. *Proc Roy Soc A* 1977;357:453.
- [35] Li J. *Model Simul Mater Sci Eng* 2003;11:173.